

# A guiding vector field algorithm for path following control of nonholonomic mobile robots

Yuri A. Kapitanuyk, Anton V. Proskurnikov and Ming Cao

**Abstract**—In this paper we propose an algorithm for path-following control of the nonholonomic mobile robot based on the idea of the *guiding vector field*. The desired path may be an arbitrary smooth curve in its implicit form, that is, a level set of some known smooth function. Using this function and the kinematic robot’s model, we design a guiding vector field, whose integral curves converge to the trajectory. A nonlinear motion controller is then proposed which steers the robot along such an integral curve, bringing it to the desired path. We give conditions for the *global* convergence of our algorithm. Experiments with real wheeled robots confirm the applicability and performance of the proposed path following control algorithm.

**Index Terms**—Path following, vector field guidance, mobile robot, motion control, nonlinear systems

## I. INTRODUCTION

Many applications in industrial and mobile robotics employ algorithms for following accurately a predefined geometric path [1], [2]. In particular, path following is one of the central problems in automatic guidance of unmanned mobile robots, such as aerial [3] and underwater [4] vehicles, wheeled ground robots [5], autonomous cars [6] and surface marine crafts [7]. In spite of substantially different mathematical models of robots, the approaches to their path-following control are similar and can be classified in several major categories.

One approach to steer to the desired path is to fix its time-parametrization; the path is thus treated as a function of time or, equivalently, the trajectory of some reference point. Path steering is then reduced to reference-point following, which is a special case of the *reference tracking* problem that has been extensively studied in control theory and solved for a very broad class of nonlinear systems [8], [9]. An obvious advantage of the trajectory tracking approach is its applicability to a broad range of paths that can be e.g. non-smooth or self-intersecting. However, this method has serious unavoidable limitations as well, especially when dealing with general nonlinear systems. As shown in [10], unstable zero dynamics generally make it impossible to trace a reference trajectory with arbitrary predefined accuracy; more precisely, the integral tracking error is uniformly positive independent

of the controller design. Furthermore, in practice the robot’s motion along the track can be quite “irregular” due to its oscillations around the reference point. For instance, it is impossible to guarantee either path following at a precisely constant speed, or even the motion with a perfectly fixed direction. Attempting to keep close to the reference point, the robot may “overtake” it due to unpredicted disturbances.

As has been clearly illustrated in the influential paper [11], these performance limitations of trajectory tracking can be removed by carefully designed *path following* algorithms. Unlike the tracking approach, path following control treats the path as a geometric curve rather than a function of time, dealing with its implicit equations or some time-free parametrization. The algorithm thus becomes “flexible to use a timing law as an additional control variable” [11]; this additional degree of freedom allows to maintain a constant forward speed or any other desired speed profile, which is extremely important e.g. for aerial vehicles, where the lifting force depends on the robot’s speed. The *dynamic* controller, maintaining the longitudinal speed, is usually separated from “geometric” controller, steering the robot to the desired path.

A widely used approach to path-following, originally proposed for car-like wheeled robots [5], [12], assumes the existence of the *projection* point, that is, the the closest point on a path, and the robot’s capability to measure the distance to it (sometimes referred to as the “cross-track error”). The robot’s mathematical model is represented in the Serret-Frenet frame, consisting of the tangent and normal vector to the trajectory at the projection point. This representation allows to design efficient path following controllers for autonomous wheeled vehicles [5], [6], [12] that eliminate the cross-track error and maintain the desired vehicle’s speed along the path. Further development of this approach leads to algorithms for the control of complex unmanned vehicles such as cars with multiple trailers [13] and agricultural tractors [14]. Projection-based *sliding mode* algorithms [6], [14] are capable to cope with uncertainties, caused by the non-trivial geometry of the path, lateral drift of the vehicle and actuator saturations.

The necessity to measure the distance to the track imposes a number of limitations on the path-following algorithm. Even if the nearest point is unique, the robot should either be equipped with special sensors [6] or solve real-time optimization problems to find the cross-track error. In general, the projection point cannot be uniquely determined when e.g. the robot passes a self-intersection point of the path or its position is far from the desired trajectory. A possible way to avoid these difficulties has been suggested in [15] and is referred to as the “virtual target” approach. The Serret-Frenet

The work was supported by the European Research Council (ERCStG-307207), RFBR, grant 14-08-01015, and St. Petersburg State University, grant 6.38.230.2015. Theorem 1 was obtained under sole support of Russian Science Foundation (RSF), grant 14-29-00142 at IPME RAS.

Yuri Kapitanuyk and Ming Cao are with the ENTEG institute at the University of Groningen, The Netherlands.

Anton V. Proskurnikov is with the ENTEG institute at the University of Groningen, The Netherlands, and also with St. Petersburg State University, Institute for Problems of Mechanical Engineering of Russian Academy of Sciences (IPME RAS) and ITMO University, St. Petersburg, Russia

E-mail: {i.kapitaniuk, a.v.proskurnikov, m.cao}@rug.nl

frame, assigned to the projection point in the algorithm from [5], [12], can be considered as the body frame of a *virtual target vehicle* to be tracked by the real robot. A modification of this approach, offered in [15], allows the virtual target to have its own dynamics, taken as one of the controller's design parameter. The design from [15] is based on the path following controller from [12], using the model representation in the Serret-Frenet frame and taking the geometry of the path into account. However, the controller from [15] implicitly involves target tracking since the frame has its own dynamics. Avoiding the projection problem, the virtual target approach thus inherits disadvantages of the usual target tracking. In presence of uncertainties the robot may slow down and turn back in order to trace the target's position [3].

A guidance strategy of a human helmsman inspired another path following algorithm, referred to as the *line-of-sight* (LOS) method [3], [7], [16] which is primarily used for air and marine crafts. Maintaining the desired speed of the robot, the LOS algorithm steers its heading along the LOS vector which starts at the robot's center of gravity and ends at the *target* point. This target is located ahead of the robot either on the path [3] or on the line, tangent to the path at the projection point [7]. Unlike the virtual target approach, the target is always chosen at a fixed prescribed distance from the robot, referred to as the *lookahead distance*. The maneuvering characteristics substantially depend on the lookahead distance: the shorter distance is chosen, the more "aggressive" it steers. A thorough mathematical examination of the LOS method has been carried out in the recent paper [7], establishing the uniform semi-global exponential stability (USGES) property.

Differential-geometric methods for invariant sets stabilization [8], [9], [17] have given rise to a broad class of "set-based" [18] path following algorithms. Treating the path as a geometric set, the algorithm is designed to make it invariant and attractive (globally or locally). Typically the path is considered as a set where some (nonlinear) output of the system vanishes, and thus the problem of its stabilization boils down to the output regulation problem. To solve it, various linearization techniques have been proposed [17], [19]–[25]. For stabilization of a closed *strictly convex* curve an elegant passivity-based method has been established in [18].

In this paper we develop a path following strategy, based on the idea of reference *vector field*. Vector field algorithms are widely used in collision-free navigation problems [26], [27]. The efficiency in path following problems has been demonstrated in recent papers [3], [28]–[30]. These methods assume that in some domain, containing the desired path, a vector field is defined whose integral curves approach the path (being itself an integral curve) asymptotically. To drive the robot to the desired path, the control algorithm steers it along the integral curves and drives it thus to the desired path from any point of the domain. Unlike many path following algorithms, providing convergence only in a *sufficiently small* vicinity of the desired path, the vector field algorithm guarantees convergence of any trajectory, which does not encounter the "critical" points where the vector field is undefined; hence, one can prove convergence in any invariant domain without critical points.

For holonomic robots described by a single or double

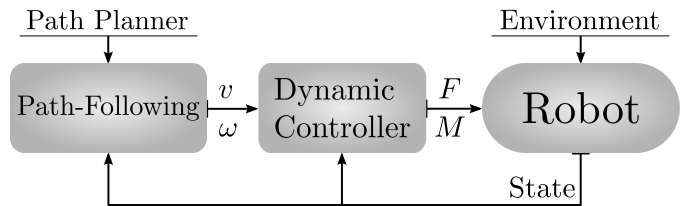


Fig. 1. The structure of motion control systems

integrator model a general vector-field algorithm for navigation along a general smooth curve in  $n$ -dimensional space has been discussed in [31]. However, for more realistic nonholonomic vehicles the vector-field algorithms have been studied only for straight line and circular paths [28], [29], [32], where they demonstrate better, in several aspects, performance compared to other approaches [3]. Unlike [3], [28], [29], in this paper we propose a vector-field algorithm for guidance of a general nonholonomic robot along a *general curvilinear path* on the plane, given in its implicit form, and give its rigorous mathematical analysis by using a special Lyapunov function.

The paper is organized as follows. The path following problem is set up in Section II, and Section III offers the vector field algorithm for path following and establishes its main properties. This algorithm is practically validated by experiments with wheeled robots, described in Section IV. Main results are proved in Section V.

## II. PROBLEM SETUP

A widely used paradigm in path following control is to decompose the controller into an "inner" and an "outer" feedback loops [33]–[35] as illustrated in Fig. 1. The "inner" *dynamic* controller is responsible for maintaining the vector of generalized velocities (e.g. the longitudinal speed and turn rate) by controlling the vector of forces and moments. The design of the dynamic controller is based on the robot's mathematical model and may include rejection of external disturbances, e.g. adaptive drift compensators [36]. Assuming the dynamic controller to be sufficiently fast and precise, one may consider the speed and the turn rate to be new control inputs, describing thus the robot with a simpler *kinematic* model. The path following algorithm is typically implemented in the "outer" *kinematic* controller, steering the simplified kinematic model to the prescribed path.

The kinematic model of a mobile robot can be *holonomic* or *nonholonomic*. A holonomic robot is not restricted by its angular orientation and able to move in any direction, as exemplified by helicopters, wheeled robots with omnidirectional wheels [2] and fully actuated marine vessels at low speeds [16]. For nonholonomic robots only some directions of motion are possible. The simplest model of this type is *unicycle*, which can move only in longitudinal direction while the lateral motion is impossible. Many practically applications, including differential drive wheeled mobile robots [13], [37], fixed wing aircraft [28], [29], [34], marine vessels at cruise speeds [33] can be reduced, under certain conditions, to the unicycle-type kinematics. The same holds for car-like vehicles [13], [20], [37], assuming that only the front wheels are

steerable. The most interesting are unicycle models where the speed is restricted to be sufficiently high, making it impossible to reduce the unicycle to a holonomic model via the feedback linearization [38]. The lift force of a fixed-wing UAV, the rudder's yaw moment of a marine craft and the turn rate of a car-like robot depend on the longitudinal speed; at a low speed the manoeuvrability of such robots is lost or very limited.

In this paper, we consider the unicycle-type model where the longitudinal velocity is a predefined constant  $u_r > 0$ .

$$\dot{\bar{r}} = \begin{bmatrix} \dot{x} \\ \dot{y} \end{bmatrix} = u_r \bar{m}(\alpha), \quad \bar{m}(\alpha) = \begin{bmatrix} \cos \alpha \\ \sin \alpha \end{bmatrix}, \quad (1)$$

$$\dot{\alpha} = \omega. \quad (2)$$

Here  $\bar{r} = (x, y)^\top \in \mathbb{R}^2$  stands for the position of the robot's center of gravity  $C$  in the inertial Cartesian frame of reference  $OXY$ ,  $\alpha$  is the robot's orientation in this frame and  $\bar{m}(\alpha)$  is the unit orientation vector (see Fig. 2). We assume the angular velocity  $\omega$  to be the only control input to the system, so the model becomes underactuated.

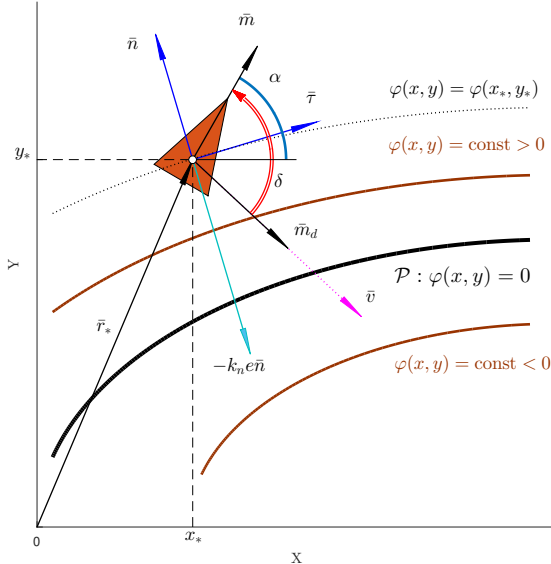


Fig. 2. The robot orientation and level sets of the function  $\varphi(x, y)$

A curvilinear desired path  $\mathcal{P} \subset \mathbb{R}^2$  is described by the implicit equation

$$\mathcal{P} = \{(x, y) : \varphi(x, y) = 0\} \quad (3)$$

where the function  $\varphi : \mathbb{R}^2 \rightarrow \mathbb{R}$  is  $C^2$ -smooth. The same geometric curve  $\mathcal{P}$  may be represented in the implicit form (3) in many ways. The principal restrictions imposed by our approach is *regularity*: in some vicinity of  $\mathcal{P}$  one has [17]

$$\nabla \varphi(x, y) = \left[ \frac{\partial \varphi(x, y)}{\partial x}; \frac{\partial \varphi(x, y)}{\partial y} \right]^\top \neq 0. \quad (4)$$

As illustrated in Fig. 2, the plane  $\mathbb{R}^2$  is covered by the disjoint *level sets* of the function  $\varphi$  that is, the sets where  $\varphi(x, y) = c = \text{const}$ . The path is one of the level sets,

corresponding to  $c = 0$ ; the value  $\varphi(x(t), y(t))$  can be considered as a (signed) “distance” from the robot to the path (differing, as usual, from the Euclidean distance).

Generally, consider a strictly increasing  $C^1$ -function  $\psi : \mathbb{R} \rightarrow \mathbb{R}$  with  $\psi(0) = 0$  (and thus  $\psi(s)s > 0$  for any  $s \neq 0$ ). One may treat

$$e = \psi[\varphi(x, y)] \in \mathbb{R}, \quad (5)$$

as the *tracking error* [17], [22]. By definition,  $e = 0$  if and only if  $(x, y) \in \mathcal{P}$ . Our goal is to design a path following algorithm, i.e. a causal feedback law  $(x(\cdot), y(\cdot), \alpha(\cdot)) \mapsto \omega(\cdot)$ , which eliminates the tracking error  $|e(t)| \xrightarrow{t \rightarrow \infty} 0$ , bringing thus the robot to the predefined path  $\mathcal{P}$ . From (1) and (2), upon reaching the desired path, the robot follows it at the constant speed  $u_r > 0$ , whereas its heading is steered along the tangent vector to the path.

The mapping  $\psi(\cdot)$  in (5) is a free parameter of the algorithm. Formally one can get rid of this parameter, replacing  $\varphi$  by the composition  $\psi \circ \varphi$ . However, it is convenient to distinguish between the path-defining function  $\varphi(x, y)$  and the tracking error, depending on the choice of  $\psi(s)$ . The path representation is usually chosen as simple as possible: for instance, dealing with a straight line, it is natural to choose  $\varphi(x, y)$  linear, while the circular path is naturally described by  $\varphi(x, y) = (x - x_0)^2 + (y - y_0)^2$ . At the same time, some mathematical properties of the algorithm, in particular, the region where convergence of the algorithm is guaranteed, depend on the way the tracking error is calculated. As will be discussed, it may be convenient to choose  $\psi(\cdot)$  bounded with  $|\psi'(s)| \xrightarrow{|s| \rightarrow \infty} 0$ , for instance,  $\psi(s) = \arctan s^p$  or  $\psi(s) = |s|^p \text{sign } s / (1 + |s|^p)$  with  $p \geq 1$ . The mentioned two functions, as well as the simplest function  $\psi(s) = s$  satisfy the condition, which we always assume to hold

$$\sup_{u \in \mathbb{R}} |\psi'(\psi^{-1}(u))| < \infty. \quad (6)$$

**Remark 1.** To focus on the ideas of the path following algorithm, we confine ourselves to the simplest nonholonomic model (1), (2). It does not take into account external disturbances, unavoidable in practice and leading to the lateral drift. The navigation algorithm from this paper can be extended to more general models, involving such a drift (e.g. by enhancing heading controller with an adaptive drift compensator, as done for the LOS method in [36]). Furthermore, our approach can be extended to the case of 3D path-following and time-varying paths (or, alternatively, moving frames), some results in these directions are reported in [24].

### III. MAIN RESULT: CONTROLLER DESIGN

We start with introducing some notation. At any point  $(x_*, y_*)$ , where (4) holds,  $\bar{n} = \nabla \varphi(x_*, y_*)$  is a normal vector to the level curve  $\varphi(x, y) = \varphi(x_*, y_*)$ , and the unit tangent vector  $\bar{\tau} = \bar{\tau}(x_*, y_*)$  is chosen in a way that the basis  $(\bar{\tau}; \bar{n})$  is right-handed oriented<sup>1</sup> (Fig. 2)

$$\bar{n}(x_*, y_*) = \nabla \varphi(x_*, y_*), \bar{\tau}(x_*, y_*) = E \bar{n}(x_*, y_*), E = \begin{bmatrix} 0 & 1 \\ -1 & 0 \end{bmatrix}.$$

<sup>1</sup>Our algorithm works, replacing everywhere  $\bar{\tau}$  with  $-\bar{\tau}$ , which causes the change of the robot's direction on the path.

### A. Design of the vector field

The basic idea of the path following algorithm is to steer to a direction, decreasing the tracking error (5). Introducing the function

$$V(x, y) = \frac{1}{2}e^2(x, y), \quad (7)$$

its derivative along the solutions of (1), (2) is

$$\dot{V} = e(x, y) \psi'(\varphi(x, y)) \nabla \varphi(x, y)^\top \dot{\bar{r}} = u_r \psi'(\psi^{-1}(e)) e \bar{n}^\top \bar{m}. \quad (8)$$

If  $e \neq 0$ , the function  $V$  (and hence  $|e|$ ) is decreasing, provided that  $e \bar{n}^\top \bar{m} < 0$ . On the other hand, as  $e \approx 0$ , one has to guide the robot to steer to the path  $\mathcal{P}$  so that  $\bar{m} \approx \bar{\tau}/\|\bar{\tau}\|$ . This motivates to design the heading controller in a way to provide the desired orientation  $\bar{m} \uparrow \bar{v}$ , where the vector field  $\bar{v}$  is given by

$$\bar{v}(x, y) = \bar{\tau}(x, y) - k_n e(x, y) \bar{n}(x, y), \quad k_n = \text{const} > 0. \quad (9)$$

In other words, the desired orientation is  $\bar{m} = \bar{m}_d$ , where

$$\bar{m}_d = \frac{\bar{v}}{\|\bar{v}\|}, \quad \bar{v}(x, y) \neq 0. \quad (10)$$

We call  $\bar{m}_d(x, y)$  the *guiding vector field*. Fig. 2 illustrates the relations between the vectors  $\bar{r}$ ,  $\bar{m}$ ,  $\bar{\tau}$ ,  $\bar{n}$ ,  $\bar{v}$  and  $\bar{m}_d$ .

Given some scalar- or vector-valued function of the position and/or heading  $F(x, y, \alpha)$  and a trajectory  $(x(t), y(t), \alpha(t))$  of the robot, we will denote, with some abuse of notation,  $F(x(t), y(t), \alpha(t))$  with  $F(t)$  and  $\frac{d}{dt}F(x(t), y(t), \alpha(t))$  with  $\dot{F}(t)$ .

The controller offered in the next subsection employs the field vector  $\bar{m}_d(x, y)$  at any point as well as its derivative along the trajectory  $\dot{\bar{m}}_d$ . Differentiating (9), one arrives at

$$\dot{\bar{v}} = u_r [E - I_2 k_n e(x, y)] H(x, y) \bar{m}(\alpha) - u_r k_n \dot{e} \bar{n}(x, y), \quad (11)$$

$$\dot{e} = \psi'(\varphi(x, y)) \bar{n}(x, y)^\top \bar{m}(\alpha), \quad (12)$$

$$\dot{\bar{m}}_d = \frac{d}{dt} \frac{\bar{v}}{\|\bar{v}\|} = \left( \frac{I_2}{\|\bar{v}\|} - \frac{\bar{v} \bar{v}^\top}{\|\bar{v}\|^3} \right) \dot{\bar{v}}. \quad (13)$$

Here  $I_2$  is  $2 \times 2$  identity matrix and  $H$  stands for the Hessian

$$H(x, y) = \begin{bmatrix} \frac{\partial^2}{\partial x^2} \varphi(x, y) & \frac{\partial^2}{\partial x \partial y} \varphi(x, y) \\ \frac{\partial^2}{\partial x \partial y} \varphi(x, y) & \frac{\partial^2}{\partial y^2} \varphi(x, y) \end{bmatrix}.$$

Since  $\|\bar{m}_d\|^2 = 1$ , one has  $\bar{m}_d^\top \dot{\bar{m}}_d = 0$ , and hence  $\dot{\bar{m}}_d = -\omega_d E \bar{m}_d$ , where  $\omega_d = \omega_d(x, y, \alpha) = -\dot{\bar{m}}_d^\top E \bar{m}_d$  is a scalar function that can be explicitly found from (11)-(13).

### B. Path following controller design

As was discussed in the foregoing, the idea of the path following algorithm is to steer the robot's orientation along the guiding vector field  $\bar{m}_d = \bar{m}_d(x, y)$ . We introduce the directed angle  $\delta = \delta(x, y, \alpha) \in (-\pi; \pi]$  between  $\bar{m}_d$  and  $\bar{m}$  (see Fig. 2). The function  $\delta(x, y, \alpha)$  is thus defined for any triple  $(x, y, \alpha)$ , being  $C^1$ -smooth on the set of points where  $\bar{m}(\alpha) \neq -\bar{m}_d(x, y)$ .

Obviously, the vector  $\bar{m}$  can be decomposed as follows

$$\bar{m} = (\cos \delta) \bar{m}_d - (\sin \delta) E \bar{m}_d. \quad (14)$$

As was noticed,  $\dot{\bar{m}} = -\omega E \bar{m}$ , whereas  $\dot{\bar{m}}_d = -\omega_d E \bar{m}_d$ . By noticing that  $\sin \delta = -\bar{m}^\top E \bar{m}_d$  and  $\cos \delta = \bar{m}^\top \bar{m}_d$ , at any time  $t \geq 0$  when  $\bar{m}(\alpha(t)) \neq -\bar{m}_d(x(t), y(t))$  (that is,  $\delta < \pi$ ) one has

$$-\omega E \bar{m} = \dot{\bar{m}} = -\dot{\delta} E \bar{m} - \omega_d E \bar{m}_d \iff \dot{\delta} = \omega - \omega_d. \quad (15)$$

More generally, at any time the following equality is valid

$$\frac{d}{dt} \sin \delta = -\frac{d}{dt} \bar{m}^\top E \bar{m}_d = (\omega - \omega_d) \cos \delta. \quad (16)$$

Supposing that  $\delta(t_0) = \pi$  and  $\omega(t) - \omega_d(t) \leq 0$  for  $t \approx t_0$ , equation (16) entails that  $\sin \delta \geq 0$  and hence  $\delta = \frac{\pi}{2} + \arcsin(\sin \delta)$  for  $t \in [t_0; t_0 + \varepsilon)$ , where  $\varepsilon > 0$  is sufficiently small. Thus, in spite of its discontinuity, the function  $\delta(x(t), y(t), \alpha(t))$  has the right derivative<sup>2</sup>  $\dot{\delta} = D^+ \delta$ , satisfying (15) as  $t \in [t_0; t_0 + \varepsilon)$ .

We are now in position to describe our path-following algorithm. Calculating  $\omega_d(x(t), y(t), \alpha(t))$  at any point, the control input is

$$\boxed{\omega(t) = \omega_d(x(t), y(t), \alpha(t)) - k_\delta \delta(x(t), y(t), \alpha(t))}. \quad (17)$$

Here  $k_\delta > 0$  is a constant, determining the convergence rate.

When  $\delta(x(t), y(t), \alpha(t)) < \pi$ , equality (15) holds and thus

$$\boxed{\dot{\delta} = \omega - \omega_d = -k_\delta \delta}. \quad (18)$$

Furthermore, even for  $\delta(x(0), y(0), \alpha(0)) = \pi$  one has  $\omega - \omega_d = -k_\delta \delta < 0$  as  $t \approx t_0$  and hence (18) retains its validity at  $t = 0$ , treating  $\dot{\delta}$  as the right derivative  $D^+ f$ . Thus, considering  $\dot{\delta}$  as a new control input, the algorithm (15) is equivalent to a very simple proportional controller (18), which implies, in particular, that if  $\delta(x(t), y(t), \alpha(t)) < \pi$  except for, possibly,  $t = 0$ .

### C. Properties of the solutions

In this subsection we establish our main results, concerned with the properties of the solutions of the closed-loop system

$$\begin{aligned} \dot{x}(t) &= u_r \cos \alpha(t), \quad \dot{y}(t) = u_r \sin \alpha(t), \\ \dot{\alpha}(t) &= \omega_d(x(t), y(t), \alpha(t)) - k_\delta \delta(x(t), y(t), \alpha(t)). \end{aligned} \quad (19)$$

The right-hand side of (19) is continuous at any point  $(x_0, y_0, \alpha_0)$ , where  $\bar{n}(x_0, y_0) \neq 0$  and  $\delta_0 = \delta(x_0, y_0, \alpha_0) < \pi$ . However, the discontinuity at the points where  $\delta_0 = \pi$  makes the usual existence theorem [39] inapplicable. To cope with this, we consider the system

$$\begin{aligned} \dot{x}(t) &= u_r \cos(t), \quad \dot{y}(t) = u_r \sin \alpha(t), \\ \dot{\alpha}(t) &= \omega_d(x(t), y(t), \alpha(t)) - k_\delta \delta_*(t), \\ \dot{\delta}_*(t) &= -k_\delta \delta_*(t). \end{aligned} \quad (20)$$

As was discussed in the previous subsection, any solution of (19) satisfies (20), where  $\delta_*(t) = \delta(x(t), y(t), \alpha(t))$ , and vice versa: choosing a solution  $\bar{r}(t), \alpha(t), \delta_*(t)$ , where  $\delta_*(0) = \delta(x(0), y(0), \alpha(0)) \in (-\pi; \pi]$ , the angle  $\delta$  satisfies (18) and

<sup>2</sup>By definition, the right derivative of a function  $f(t)$  at  $t = t_0$  (written  $f'(t_0 + 0)$  or  $D^+ f(t_0)$ ) is defined by  $D^+ f(t_0) = \lim_{t \rightarrow t_0 + 0} \frac{f(t) - f(t_0)}{t - t_0}$ .

hence  $\delta_*(t) = \delta(x(t), y(t), z(t))$ . Unlike the closed-loop system (19), the right-hand side of (20) is a  $C^1$ -smooth function of  $(x, y, \alpha, \delta_*)$  at any point where  $\bar{n}(x, y) \neq 0$ . Applying the standard existence and uniqueness theorems [39] to (20), one arrives at the following.

**Lemma 1.** *For any point  $\zeta_0 = (x_0, y_0, \alpha_0)$ , such that  $\bar{n}(x_0, y_0) \neq 0$ , there exists the unique solution  $\zeta(t) = (x(t), y(t), \alpha(t))$  with  $\zeta(0) = \zeta_0$ . Extending this solution to the maximal existence interval  $[0; t_*)$ , one either has  $t_* = \infty$  (the solution is infinitely prolongable) or  $t_* < \infty$  and  $(x(t), y(t)) \xrightarrow[t \rightarrow t_*]{} (x_*, y_*)$ , where  $|\bar{n}(x_*, y_*)| = 0$ .*

To prove the basic properties of the solutions, we adopt several technical assumptions, needed to avoid some “pathological” situations. Recall that the desired path  $\mathcal{P}$  is a level set  $\{\varphi(x, y) = 0\}$  (or, equivalently,  $e = 0$ ). To use  $e(x, y)$  as analog of “signed distance” to the path  $\mathcal{P}$ , the convergence  $e(x(t), y(t)) \xrightarrow[t \rightarrow \infty]{} 0$  should provide that the robot asymptotically approaches  $\mathcal{P}$ , that is, the Euclidean distance<sup>3</sup>  $\text{dist}(\bar{r}(t), \mathcal{P}) \xrightarrow[t \rightarrow \infty]{} 0$ . When  $\mathcal{P}$  is a closed curve, it suffices to assume that  $e(x, y)$  does not vanish as  $|\bar{r}| \rightarrow \infty$ . For a general path  $\mathcal{P}$ , which may be unbounded, we adopt the following assumption.

**Assumption 1.** *For arbitrarily small positive  $\varkappa > 0$  one has*

$$\inf\{|e(\bar{r})| : \text{dist}(\bar{r}, \mathcal{P}) \geq \varkappa\} > 0. \quad (21)$$

Our next two assumptions are concerned with the behavior of the normal vector  $\bar{n} = \nabla\varphi$ , which determines the vector field  $\bar{m}_d$ . The second assumption provides the existence of the field (and thus applicability of our algorithm) in a small vicinity of the path.

**Assumption 2.** *The set of critical points, where  $\bar{n}$  vanishes,*

$$\mathcal{C}_0 = \{\bar{r} = (x, y) : \nabla\varphi(\bar{r}) = 0\},$$

*is bounded (and hence compact) and does not intersect the desired path  $\mathcal{C}_0 \cap \mathcal{P} = \emptyset$ . Since the set  $\mathcal{P}$  is closed, this implies in fact that  $\mathcal{P}$  and  $\mathcal{C}_0$  are separated by a positive distance  $\text{dist}(\mathcal{C}_0, \mathcal{P}) > 0$ .*

Our last assumption restricts the asymptotical behavior of the normal vector at infinity. This assumption is technical and may be relaxed, however, we adopt it in order to prove the results for bounded and unbounded paths in a simpler and unified way.

**Assumption 3.** *There exist  $\theta \in (0; k_\delta)$  and  $C_1, C_2 > 0$  such that*

$$C_1 \leq |\bar{n}(\bar{r})| \leq C_2 e^{\theta|\bar{r}|} \quad \text{as } |\bar{r}| \rightarrow \infty. \quad (22)$$

**Remark 2.** *The first inequality in (22) implies that the norm  $|\bar{n}(\bar{r})|$  is uniformly positive over any closed set without critical points. In other words,  $\inf\{|\bar{n}(\bar{r})| : \text{dist}(\bar{r}, \mathcal{C}_0) \geq \varkappa\} > 0$ .*

<sup>3</sup>As usual, the distance from a point  $\bar{r}_0$  to the path  $\mathcal{P}$  is  $\text{dist}(\bar{r}_0, \mathcal{P}) = \inf\{|\bar{r}_0 - \bar{r}| : \bar{r} \in \mathcal{P}\}$ . More generally, the distance between sets  $A, B$  is defined as  $\text{dist}(A, B) = \inf\{|r_1 - r_2| : r_1 \in A, r_2 \in B\}$ .

**Remark 3.** *The second inequality in (22), obviously, remains valid for arbitrary point  $\bar{r}$ , choosing  $C_2$  sufficiently large. It entails, in particular, that the function  $|\bar{n}(x(t), y(t))|e^{-k_\delta t} \xrightarrow[t \rightarrow \infty]{} 0$  exponentially. Recalling that the angle  $\delta$  between the unit vectors  $\bar{m}$  and  $\bar{m}_d$  obeys (18), this implies the exponential decaying of  $\bar{n}^\top(\bar{m} - \bar{m}_d)$ , which allows to estimate the right-hand side in (8).*

We are now in position to formulate our first main result.

**Theorem 1.** *Let Assumptions 1-3 hold. Then for any maximally prolonged solution  $\zeta(t) = (x(t), y(t), \alpha(t))$ ,  $t \in [0; t_*)$ , either*

- 1)  $t_* = \infty$  and  $\text{dist}(\bar{r}(t), \mathcal{P}) \xrightarrow[t \rightarrow \infty]{} 0$ , or
- 2)  $\text{dist}(\bar{r}(t), \mathcal{C}_0) \rightarrow 0$  as  $t \rightarrow t_*$  (where  $t_*$  can be finite or infinite).

*In other words, for any initial condition the algorithm drives the robot to the desired path, unless it “gets stuck” at one of the critical points (or converges to it asymptotically).*

**Corollary 1.** *Suppose that  $\mathcal{C}_0 = \emptyset$  and Assumptions 1 and 3 hold. Then any solution is infinitely prolongable and the algorithm provides the asymptotic path following  $\text{dist}(\bar{r}(t), \mathcal{P}) \xrightarrow[t \rightarrow \infty]{} 0$ .*

Corollary 1 is applicable to linear mappings  $\varphi(x, y) = ax + by + c$  (with  $|a| + |b| \neq 0$ ) and many other functions, e.g.  $\varphi(x, y) = y + f(x)$ . These functions, however, usually correspond to unbounded desired curves (e.g., linear functions describe straight lines). When the goal is to circulate along some closed curve, the corresponding normal vector  $\bar{n} = \nabla\varphi(x, y)$  typically degenerates at some points ( $\mathcal{C}_0 \neq \emptyset$ ).

In practice,  $\mathcal{C}_0$  often consists of isolated critical points and experiments show that the robot “evades” them, so the second alternative in Theorem 1 is never realized. The mathematical conditions for this, however, are inevitably conservative and guarantee convergence in some invariant set, free of critical points. Notice that similar restrictions naturally arise in projection-based algorithms, where convergence can be rigorously proved only in some region of attraction where the projection to the desired curve is well defined [14].

We are now going to describe explicitly a large invariant set without critical points, containing the desired path  $\mathcal{P}$ . Assumptions 1 and 2 entail that the tracking error is uniformly positive on  $\mathcal{C}_0$ , that is,

$$e_c = \inf\{|e(x, y)| : (x, y) \in \mathcal{C}_0\} > 0. \quad (23)$$

We introduce the set

$$\mathcal{M} = \{(x, y, \alpha) : \bar{n} \neq 0, |\delta| < \arctan(k_n e_c), |e| < e_c\}. \quad (24)$$

Recall that  $k_n$  is the constant parameter from (9) and  $\delta = \delta(x, y, \alpha)$  is the angle between the robot’s heading and the vector field direction. By definition,  $\mathcal{M} \cap \mathcal{C}_0 = \emptyset$ . The following lemma states that in fact  $\mathcal{M}$  is an invariant set, i.e. any solution starting at  $\mathcal{M}$  remains there.

**Theorem 2.** *Consider a solution  $(x(t), y(t), \alpha(t))$ , starting at  $(x(0), y(0), \alpha(0)) \in \mathcal{M}$ . Then the solution is infinitely prolongable and  $(x(t), y(t), \alpha(t)) \in \mathcal{M} \forall t \geq 0$ . Moreover,*

at any point  $t \geq 0$  the tracking error  $e(t) = e(x(t), y(t))$  satisfies the inequality

$$|e(t)| \leq \max\{|e(0)|, k_n^{-1} \tan \delta(0)\} < e_c. \quad (25)$$

Under Assumptions 1-3 algorithm (17) enables following asymptotically the desired path  $\text{dist}(\bar{r}(t), \mathcal{P}) \xrightarrow{t \rightarrow \infty} 0$ .

**Remark 4.** The condition  $(x(0), y(0), \alpha(0)) \in \mathcal{M}$  restricts the robot to be “properly” headed in the sense that its initial orientation relative to the vector field  $\delta(0) = \delta(x(0), y(0), \alpha(0))$  satisfies

$$|\delta| < \arctan(k_n e_c) < \pi/2. \quad (26)$$

Since  $e_c > 0$ , (26) is valid for sufficiently large  $k_n$  whenever  $|\delta| < \pi/2$ . In other words, Theorem 2 guarantees convergence to the path from any starting position with  $|e(0)| < e_c$  and  $|\delta(0)| < \pi/2$ , choosing  $k_n$  large. Furthermore, if the desired path  $\mathcal{P}$  is closed and the direction of circulation along it is unimportant, the condition  $|\delta(0)| < \pi/2$  can be provided by reverting the vector field  $\bar{m}_d \mapsto -\bar{m}_d$  (which corresponds to the replacement of  $\varphi \mapsto -\varphi$  and  $|\delta| \mapsto \pi - |\delta|$ ) unless  $\delta(0) = \pm\pi/2$  (in practice is never possible).

**Remark 5.** Even if (26) is violated at the starting time  $t = 0$ , it obviously holds when  $t > t_0 = k_\delta^{-1}[\ln |\delta(0)| - \ln \arctan(k_n e_c)]$  thanks to (18). Thus, if one is able to prove that the solution is prolongable up to  $t_0$  and  $|e(x(t_0), y(t_0))| < e_c$ , Theorem 2 provides the convergence of the robot’s position to the desired path.

Remark 5 suggests the way to estimate explicitly the set of initial conditions, from where convergence to the desired path is guaranteed. Since the robot moves at the constant speed  $u_r > 0$ , it covers the distance  $u_r t_0$  until its orientation satisfies (26). The path following is guaranteed if  $u_r t_0$  is less than the viability distance of the initial position, i.e. the distance from it to the set where  $|e| \geq e_c$ .

**Definition 1.** Given a point  $\bar{r}_0 = (x_0, y_0)$  with  $|e(\bar{r}_0)| < e_c$ , we define its viability distance to be  $d_0 = \inf\{\text{dist}(\bar{r}_0, \bar{r}) : e(\bar{r}) \geq e_c\}$ .

Theorem 2 and Remark 5 yield in the following.

**Corollary 2.** Let the initial position of the robot  $\bar{r}(0) = (x(0), y(0))$  with  $e(\bar{r}(0)) < e_c$  correspond to the viability distance  $d_0 > 0$ . Suppose also that its orientation  $\alpha(0)$  satisfies the condition

$$d_0 > \frac{u_r}{k_\delta} \ln \frac{|\delta(x(0), y(0), \alpha(0))|}{\arctan(k_n e_c)}. \quad (27)$$

Then the solution of the closed-loop system gets into the set  $\mathcal{M}$  in finite time, and the algorithm (17) provides the path following  $\text{dist}(\bar{r}(t), \mathcal{P}) \xrightarrow{t \rightarrow \infty} 0$ . When the initial position satisfies

$$d_0 > \frac{u_r}{k_\delta} \ln \frac{\pi}{\arctan(k_n e_c)}, \quad (28)$$

the path following is provided independent of the initial orientation.

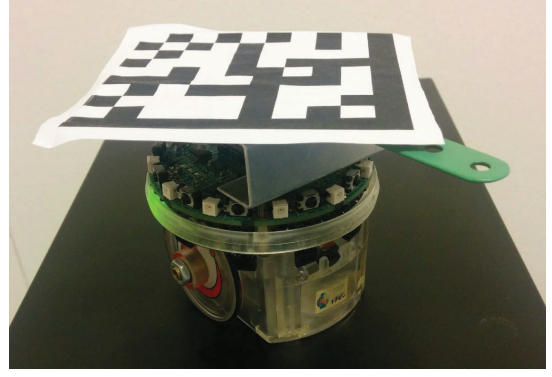


Fig. 3. The E-puck robot with marker on top, used in experiments

The condition (28) gives an estimate for the region, starting in which the robot necessarily converges to the desired path  $\mathcal{P}$ . Taking the original orientation relative to the field into account, this estimate can be tightened by using (27). Typically  $d_0$  is uniformly positive in the vicinity of  $\mathcal{P}$  (this holds, for instance, when  $\mathcal{P}$  is a closed curve). Thus (28) guarantees the algorithm to converge in the vicinity of  $\mathcal{P}$ , choosing  $k_\delta/u_r$  sufficiently large. As was mentioned, practical experiments with natural trajectories, corresponding to finite sets  $\mathcal{C}_0$ , show that the robot is always attracted to the desired path (unless starts in  $\mathcal{C}_0$ ). In Section IV the experiments with real robots are reported, where the desired path is an ellipse or Cassini oval. At the same time, mathematical proof of the convergence under “almost any” initial condition remains a non-trivial and in fact open problem.

**Remark 6.** Although explicit calculation of the viability distance is complicated, conditions (27) and (28) in fact require only its lower bound. Such a bound can be explicitly obtained, for instance, for the case where the error’s gradient is globally bounded

$$|\nabla e(x, y)| = \psi'(\varphi(x, y)) |\nabla \varphi(x, y)| \leq c = \text{const} \quad \forall x, y. \quad (29)$$

If the condition (29) holds, then  $|e(\bar{r}) - e(\bar{r}_0)| \leq c|\bar{r} - \bar{r}_0|$  and hence the viability distance of  $\bar{r}_0$  is estimated from below as follows

$$d_0 \geq (e_c - e(x_0, y_0))/c.$$

Condition (29) can often be provided under appropriate choice of  $\psi(\cdot)$ . For instance, when  $\varphi(x, y) = (x - x_0)^2 + (y - y_0)^2 - R^2$  (circular path), one can choose  $\psi(s) = \arctan s$  so that  $\psi'(s) = 1/(1+s^2)$ . More generally, when  $|\varphi(\bar{r})| \geq C_1 |\bar{r}|^\beta$  and  $|\nabla \varphi(\bar{r})| \leq C_2 |\bar{r}|^\gamma$  as  $|\bar{r}| \rightarrow \infty$ , then  $\nabla e$  is globally bounded, choosing  $\psi(s) = \arctan(s^p)$ , where  $p > 0$  is sufficiently large so that  $p - 1 + \gamma \leq 2\beta p$ .

#### IV. EXPERIMENTAL VALIDATION

We test the results using the E-puck mobile robotic platform [40]. The experimental setup consists of the differential wheeled E-puck robot, a control computer, an overhead camera and a communication module. The robot is identified by a data matrix marker on its top (see Fig. 3). The position of the

central point and the orientation of the marker are recognized by a vision algorithm running at a control computer connected to the overhead camera. The available workspace is a planar area of 2.6x2 meters covered by the image of 1280x720 Px (henceforth the acronym Px is used for pixels). For our purpose we operate with pixels as coordinates. The PC runs real-time calculation of the control actions based on the pose information of the robot and computes the control inputs for the robot. The results of computation as the desired angular and linear velocities of the robot translate into the commands for the left and right wheels. The communication is done via Bluetooth at the fixed frequency of 20 Hz. Through this wireless channel, the control computer sends the commands to the robot.

We verify the guidance algorithm for two closed trajectories, passed by the robot in *clockwise* direction. In both cases the forward velocity was set to  $u_r = 50$  Px/s, and we set parameters of the algorithm  $k_n = 3$  and  $k_\delta = 2$ . We choose  $\psi(s) = s$ , so that  $e(x, y) = \varphi(x, y)$ . Below we describe the trajectories and show the numerical data from the experiments.

#### A. Ellipse path

For our first experiment, we choose the ellipse-shaped trajectory  $\mathcal{P} : \varphi(x, y) = 0$ , where

$$\varphi(x, y) = k_s \left( \frac{(x - x_0)^2}{a^2} + \frac{(y - y_0)^2}{b^2} - R^2 \right).$$

Obviously, the level curves of  $\varphi$  are ellipses. The path  $\mathcal{P}$  corresponds to the ellipse with semiaxes  $aR$  and  $bR$ , centered at the point  $(x_0, y_0)$ .

For the experiment we choose  $x_0 = 600$ Px,  $y_0 = 350$ Px,  $R = 400$ Px, and the semiaxes scale factors  $a = 1$ ,  $b = 0.5$  (see Fig. 4). To provide  $\varphi(x, y) \in [-5; 5]$  in the working area, we choose the scaling factor  $k_s = 10^{-5}$ . The robots's trajectories (labeled  $a$ ,  $b$ ,  $c$  and  $d$ ) under four different initial conditions are shown in Fig. 4. The respective starting conditions are selected as follows

$$\begin{aligned} a : (x = 472, y = 311, \alpha = 0.0768), \\ b : (x = 30, y = 555, \alpha = 0.0278), \\ c : (x = 408, y = 369, \alpha = 2.1515), \\ d : (x = 78, y = 133, \alpha = 4.0419). \end{aligned} \quad (30)$$

(the coordinates  $x, y$  are in pixels, and  $\alpha$  is in radians). Fig. 5 illustrates the dynamics of the tracking error  $\varphi(x(t), y(t))$ .

In this example the set of critical points is  $\mathcal{C}_0 = \{(x_0, y_0)\}$ , which corresponds to  $e(x_0, y_0) = -k_s R^2$  and hence  $e_c = R^2$ . The set  $\{(x, y) : |e(x, y)| < e_c\}$  consists of all points, where

$$0 < \frac{(x - x_0)^2}{a^2} + \frac{(y - y_0)^2}{b^2} < 2R^2. \quad (31)$$

Theorem 2 guarantees that starting at any of these points with orientation, satisfying (26), the robot converges to the desired path. In the case where (26) fails, the convergence is guaranteed in a more narrow domain, specified by Corollary 2 (the viability distance can be found explicitly in this case). The practical experiments, however, show that the robot converges to the path from *any* point, except for the ellipse' center, independent of the initial robot's orientation, whereas the mathematically rigorous proof remains an open problem.

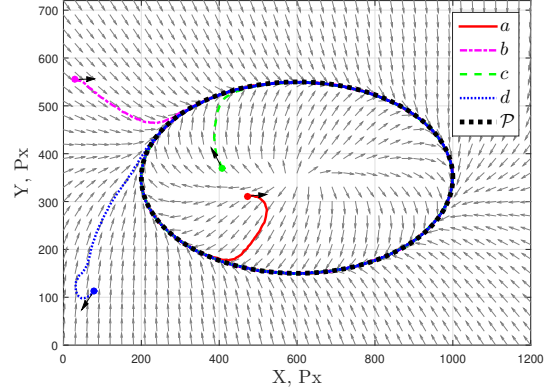


Fig. 4. Elliptical path: the vector field and robot's trajectories.

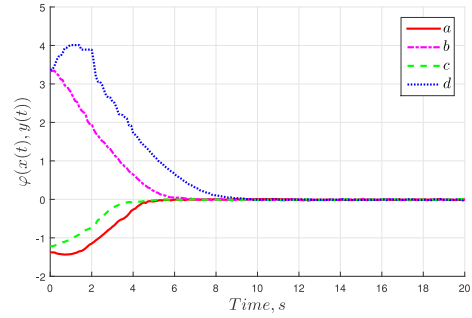


Fig. 5. Elliptical path: the dynamics of the tracking error  $e = \varphi(x, y)$ .

#### B. Circulation along the Cassini oval

For our second experiment the path chosen is referred to as the *Cassini oval* (Fig. 6) and described by the equation

$$\begin{aligned} \varphi(x, y) = k_s \left[ (\Delta x^2 + \Delta y^2)^2 - 2c^2 (\Delta x^2 - \Delta y^2) - a^4 + c^4 \right] = 0, \\ \Delta x = (x - x_0), \quad \Delta y = (y - y_0). \end{aligned}$$

We choose here  $k_s = 10^{-10}$ ,  $a = 330$ Px and  $c = 300$ Px. The oval is centered at  $(x_0, y_0) = (600, 350)$ Px.

Fig. 6 illustrates four trajectories (labeled  $a$ ,  $b$ ,  $c$  and  $d$ ), corresponding to the initial conditions

$$\begin{aligned} a : (x = 233, y = 184, \alpha = 2.9287), \\ b : (x = 106, y = 202, \alpha = 4.2487), \\ c : (x = 355, y = 343, \alpha = 5.4071), \\ d : (x = 503, y = 619, \alpha = 0.1022). \end{aligned} \quad (32)$$

(the coordinates  $x, y$  are in pixels, and  $\alpha$  is in radians). The corresponding tracking errors are displayed in Fig. 7.

## V. PROOFS OF THE MAIN RESULTS

In this section we prove Lemma 1, Theorems 1 and 2. Henceforth we assume that Assumptions 1-3 hold.

*Proof of Lemma 1:* As was discussed in Subject. III-C, the Cauchy problem for the closed-loop system (19) is equivalent to one for the system (20) with smooth right-hand side, and thus for any initial condition the solution exists locally

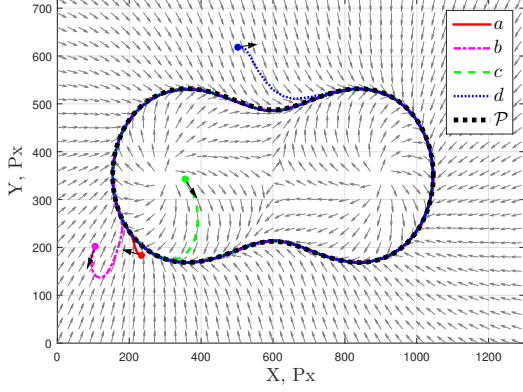


Fig. 6. Cassini oval: the vector field and robot's trajectories.

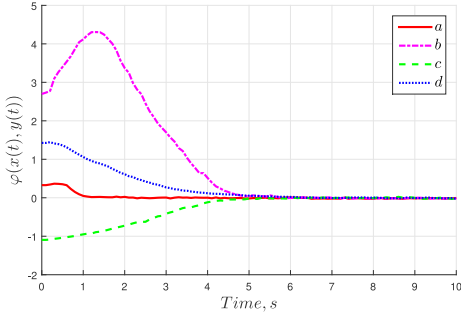


Fig. 7. Cassini oval: the dynamics of the tracking error  $e = \varphi(x, y)$ .

and is unique [39]. Let its maximal prolongation to the right  $(x(t), y(t), \alpha(t))$  be defined for  $[0; t_*)$ . Suppose that  $t_* < \infty$ . Since  $\dot{x}$  and  $\dot{y}$  are bounded, the limit

$$\bar{r}_* = \lim_{t \rightarrow t_*} \bar{r}(t) = \bar{r}(0) + \int_0^{t_*} \dot{\bar{r}}(t) dt$$

exists. Our goal is to show that  $\bar{n}(\bar{r}_*) = 0$ . Suppose, on the contrary, that  $|\bar{n}(\bar{r}_*)| > 0$ . Since  $\bar{n}$  continuously depends on  $\bar{r}$ , the same holds for  $\bar{r} \approx \bar{r}_*$  and hence  $\omega_d(x, y)$  and the right-hand side of (20) are well-defined and bounded in the vicinity of  $(x_*, y_*)$ . This enables one to define the solution at  $t = t_*$  and then, by the existence theorem, prolong it to  $[t_*, t_* + \varepsilon)$ . One arrives at the contradiction with definition of  $t_*$ , which proves that  $\bar{n}(\bar{r}_*) = 0$ . ■

To proceed with the proof of Theorem 1, we need the following technical Barbalat-type lemma.

**Lemma 2.** *Suppose the function  $\bar{r}(t) : [0; \infty) \rightarrow \mathbb{R}^2$  is absolutely continuous and  $|\dot{\bar{r}}(t)|$  is bounded. Then either  $\int_0^\infty |\bar{n}(\bar{r}(t))| dt = \infty$  or  $\text{dist}(\bar{r}(t), \mathcal{C}_0) \rightarrow 0$  and hence  $|\bar{n}(\bar{r}(t))| \rightarrow 0$  as  $t \rightarrow \infty$ .*

*Proof:* Suppose that  $\int_0^\infty |\bar{n}(\bar{r}(t))| dt < \infty$ , nevertheless  $d_\infty = \overline{\lim}_{t \rightarrow \infty} \text{dist}(\bar{r}(t), \mathcal{C}_0) > 0$ . For  $\varepsilon > 0$ , let  $\mathcal{C}_\varepsilon$  stand for the the “ $\varepsilon$ -sphere” of  $\mathcal{C}_0$ , that is, the set  $\{\bar{r} : \text{dist}(\bar{r}, \mathcal{C}_0)\} = \varepsilon$  (see Fig. 8). We choose arbitrary  $\varepsilon \in (0, d_\infty/2)$ . By definition of  $d_\infty$ , there exists a sequence  $t_n \rightarrow \infty$ , such that  $\text{dist}(\bar{r}(t_n), \mathcal{C}_0) > 2\varepsilon$ . Remark 1 implies the existence of

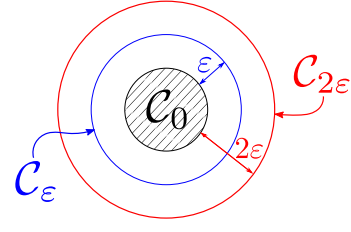


Fig. 8. Illustration to proof of Lemma 2: two “spheres” around  $\mathcal{C}_0$

another sequence  $\tilde{t}_n \rightarrow \infty$ , such that  $\text{dist}(\bar{r}(\tilde{t}_n), \mathcal{C}_0) < \varepsilon$  (otherwise, one would have  $|\bar{n}(t)| \geq \text{const} > 0$  for  $t$  sufficiently large and thus  $\int_0^\infty |\bar{n}(\bar{r}(t))| dt = \infty$ ). Passing to the subsequences, we can consider without loss of generality that  $t_n < \tilde{t}_n < t_{n+1}$ . During each interval  $[t_n, \tilde{t}_n]$  the curve  $\bar{r}(t)$  crosses thus both spheres  $\mathcal{C}_{2\varepsilon}$  and  $\mathcal{C}_\varepsilon$ . Precisely, there exist points  $t'_n$  and  $t''_n$  such that  $t_n < t'_n < t''_n < \tilde{t}_n$ ,  $\bar{r}(t'_n) \in \mathcal{C}_{2\varepsilon}$  and  $\bar{r}(t''_n) \in \mathcal{C}_\varepsilon$  and  $\text{dist}(\bar{r}(t), \mathcal{C}_0) \in (\varepsilon; 2\varepsilon)$  when  $t \in \Delta_n = (t'_n, t''_n)$ . It is obvious that the distance from a point of  $\mathcal{C}_\varepsilon$  to any point of  $\mathcal{C}_{2\varepsilon}$  is not less than  $\varepsilon$ , and thus a constant  $\tau > 0$  exists such that  $t''_n - t'_n \geq \tau$  due to boundedness of  $\dot{\bar{r}}(t)$ . Remark 2 implies now that  $|\bar{n}(\bar{r}(t))| \geq c_0 > 0$  whenever  $t \in \Delta_n$ . Since the intervals  $\Delta_j$  are disjoint, one has  $\int_{\Delta_j} |\bar{n}(\bar{r}(t))| dt \geq \tau c_0 > 0$ , so that

$$\int_0^\infty |\bar{n}(\bar{r}(t))| dt \geq \sum_{j=1}^\infty \int_{\Delta_j} |\bar{n}(\bar{r}(t))| dt = \infty.$$

One arrives at the contradiction, which proves that  $\lim_{t \rightarrow \infty} \text{dist}(\bar{r}(t), \mathcal{C}_0) = 0$ . ■

The proofs of Theorems 1 and 2 exploit the Lyapunov function (7). In view of Eqs. (8) and (14), its derivative along the trajectory is

$$\dot{V} = u_r e \psi'(\psi^{-1}(e)) [\bar{n}^\top \bar{m}_d \cos \delta - \bar{n}^\top E \bar{m}_d \sin \delta]. \quad (33)$$

Introducing the function  $\Phi(s)$  to be

$$\Phi(s) = \frac{s \psi'(\psi^{-1}(s))}{\sqrt{1 + k_n^2 s^2}},$$

condition (6) implies that  $\Phi$  is bounded. The definition of the vector field  $\bar{m}_d$  in Eqs. (9),(10) and (33) imply that

$$\dot{V} = u_r \Phi(e) |n| [-e \cos \delta + \sin \delta]. \quad (34)$$

*Proof of Theorem 1:* In accordance with Lemma 1, any solution, which is not infinitely prolongable, converges to  $\mathcal{C}_0$  in finite time. Hence it suffices to consider infinitely prolongable solutions and prove that for any of them one either has  $e(x(t), y(t)) \xrightarrow[t \rightarrow \infty]{} 0$  or  $\int_0^\infty |\bar{n}(x(t), y(t))| dt < \infty$ . Indeed, due to Assumption 1,  $e(t) \rightarrow 0$  implies that  $\text{dist}(\bar{r}(t), \mathcal{P}) \rightarrow 0$ , whereas  $\int_0^\infty \bar{n}(t) dt < \infty$  entails that  $\text{dist}(\bar{r}(t), \mathcal{C}_0) \rightarrow 0$  thanks to Lemma 2.

Recall that the deviation between the robot's heading and the vector field  $\delta(t) = \delta(x(t), y(t), \alpha(t))$  obeys (18) and hence exponentially decays  $\delta(t) = \delta(0)e^{-k_\delta t}$ . Since  $|\sin \delta| \leq |\delta|$ , Assumption 3 and condition (6) entail that  $\int_0^\infty |\Phi(e(t)) \bar{n}(t) \sin \delta(t)| dt < \infty$ . Notice now that  $(-\Phi(e)e) \leq 0$  and  $\cos \delta(t) > 0$  as  $t$  becomes sufficiently

large. Thus the integral  $\int_0^\infty (-e\Phi(e)|n|) \cos \delta dt$  exists, being either finite or equal to  $-\infty$ . This implies, thanks to (34), the existence of  $\int_0^\infty \dot{V} dt = \lim_{t \rightarrow +\infty} V(t) - V(0)$ . Since  $V \geq 0$ , the latter integral cannot equal to  $-\infty$  and thus is *finite*. This implies the existence of the finite limit  $\lim_{t \rightarrow +\infty} |e(t)|^2$  and the inequality

$$u_r \int_0^\infty e\Phi(e)|n| \cos \delta dt \leq \int_0^\infty [-\dot{V} + u_r \Phi(e(t))\bar{n}(t) \sin \delta(t)] dt < \infty.$$

Suppose that  $\lim_{t \rightarrow +\infty} |e(t)|^2 > 0$ . By definition of  $\Phi(e)$ , this implies that  $\lim_{t \rightarrow \infty} e\Phi(e) > 0$ . Since  $\delta(t) \rightarrow 0$  as  $t \rightarrow \infty$  and thus  $\cos \delta \rightarrow 1$ . This implies that  $\int_0^\infty |\bar{n}(t)| dt < \infty$ , ending the proof. ■

*Proof of Theorem 2:* Consider a trajectory  $(x(t), y(t), \alpha(t))$ , starting at the point  $(x(0), y(0), \alpha(0)) \in \mathcal{M}$ . By definition, one has  $|\delta(t)| \leq |\delta(0)| < \frac{\pi}{2}$  for any  $t$ , and hence  $\cos \delta(t) > 0$ . By noticing that  $\Phi(e)e \geq 0$ , (34) entails that  $\dot{V} \leq 0$  when  $|e| \geq |\tan \delta|$ , since

$$\dot{V} \leq -u_r |\Phi(e)| |\bar{n}| (|e| - |\tan \delta|) \cos \delta.$$

Evidently, for any solution one either has

- 1)  $|e(t)| \geq |\tan \delta(t)|$  for any  $t \geq 0$  (where the solution exists), or
- 2)  $|e(t_0)| < |\tan \delta(t_0)|$  at some  $t_0 \geq 0$ .

In the first case  $|e(t)|$  is non-increasing along the solution, and hence  $|e(t)| \leq |e(0)| < e_c$ . In the second case, we claim that  $|e(t)| \leq |\tan \delta(t_0)| \leq |\tan \delta(0)|$  for any  $t \geq t_0$ . Indeed, had we  $|e(t_1)| > |\tan \delta(t_0)|$  at some point  $t_1$ , there would exist  $t_* < t_1$  such that  $|e(t_*)| = |\tan \delta(t_0)|$  and  $|e(t)| > |\tan \delta(t_0)|$  as  $t \in (t_*, t_1]$ . The latter inequality, however, is not possible since  $|e(t)|$  is non-increasing on  $[t_*, t_1]$ . We have proved that in both cases 1) and 2) the inequality (25) holds and thus the solution stays in  $\mathcal{M}$  and, by definition (23) of  $e_c$ , the distance  $\text{dist}(\bar{r}(t), \mathcal{C}_0)$  is uniformly positive over  $t \geq 0$ . Theorem 1 now implies that  $\text{dist}(\bar{r}(t), \mathcal{P}) \xrightarrow[t \rightarrow \infty]{} 0$ . ■

## VI. CONCLUSIONS

In this paper we offer a new algorithm for path-following control of nonholonomic robots. This algorithm is based on the idea of guiding (or reference) vector field. Unlike the existing results, the desired path can be an arbitrary smooth curve in its implicit form, that is, the zero set of a smooth function. We examine mathematical properties of the algorithm and give global conditions for the following asymptotically the desired path. The results have been experimentally validated, using the E-puck wheeled robots. We are now working with our industrial partners of the EU SMARTBOT project (smartbot.eu) to implement our algorithms in industrial environments.

## REFERENCES

- [1] T. Kurfess, Ed., *Robotics and Automation Handbook*. CRC Press, 2005.
- [2] B. Siciliano and O. Khatib, Eds., *Springer Handbook of Robotics*. Springer, 2008.
- [3] P. Sujit, S. Saripalli, and J. Borges Sousa, "Unmanned aerial vehicle path following: A survey and analysis of algorithms for fixed-wing unmanned aerial vehicles," *IEEE Control Systems*, vol. 34, no. 1, pp. 42–59, 2014.
- [4] E. Peymania and T. I. Fossen, "Path following of underwater robots using Lagrange multipliers," *Robotics and Autonomous Systems*, vol. 67, pp. 44–52, 2015.
- [5] C. Samson, "Path following and time-varying feedback stabilization of a wheeled mobile robot," in *Proc. of the ICARCV'92, Singapore*, 1992.
- [6] J. Ackermann, J. Guldner, W. Siemel, R. Steinhauser, and V. I. Utkin, "Linear and nonlinear controller design for robust automatic steering," *IEEE Trans. Control Syst. Tech.*, vol. 3, no. 1, pp. 132–143, 1995.
- [7] T. I. Fossen and K. Y. Pettersen, "On uniform semiglobal exponential stability (USGES) of proportional line-of-sight guidance laws," *Automatica*, vol. 50, no. 11, pp. 2912 – 2917, 2014.
- [8] A. Isidori, *Nonlinear Control Systems*, 3rd ed., M. Thoma, E. D. Sontag, B. W. Dickinson, A. Fettweis, J. L. Massey, and J. W. Modestino, Eds. Secaucus, NJ, USA: Springer-Verlag New York, Inc., 1995.
- [9] L. Marconi and A. Isidori, "Mixed internal model-based and feedforward control for robust tracking in nonlinear systems," *Automatica*, vol. 36, no. 7, pp. 993 – 1000, 2000.
- [10] M. M. Seron, J. H. Braslavsky, P. V. Kokotovic, and D. Q. Mayne, "Feedback limitations in nonlinear systems: From Bode integrals to cheap control," *IEEE Trans. Autom. Control*, vol. 44, no. 4, pp. 829–833, 1999.
- [11] A. Aguiar, J. Hespanha, and P. Kokotovic, "Path-following for nonminimum phase systems removes performance limitations," *IEEE Trans. Autom. Control*, vol. 50, no. 2, pp. 234–239, 2005.
- [12] A. Miccaelli, C. Samson *et al.*, "Trajectory tracking for unicycle-type and two-steering-wheels mobile robots," *Tech. Rep. No. 2097, INRIA*, 1993.
- [13] C. Samson, "Control of chained systems application to path following and time-varying point-stabilization of mobile robots," *IEEE Trans. Autom. Control*, vol. 40, no. 1, pp. 64–77, 1995.
- [14] A. S. Matveev, M. Hoy, J. Katupitiya, and A. V. Savkin, "Nonlinear sliding mode control of an unmanned agricultural tractor in the presence of sliding and control saturation," *Robotics and Autonomous Systems*, vol. 61, no. 9, pp. 973 – 987, 2013.
- [15] D. Soetanto, L. Lapiere, and A. Pascoal, "Adaptive, non-singular path-following control of dynamic wheeled robots," in *Proc. of 42nd IEEE Conf. on Decision and Control*, vol. 2, Dec 2003, pp. 1765–1770 Vol.2.
- [16] M. Breivik and T. Fossen, "Principles of guidance-based path following in 2D and 3D," in *Proc. of 44th IEEE Conf. on Decision and Control and European Control Conf. CDC-ECC'05.*, Dec 2005, pp. 627–634.
- [17] A. Fradkov, I. Miroshnik, and V. Nikiforov, *Nonlinear and Adaptive Control of Complex Systems*, ser. Mathematics and Its Applications. Springer, 1999.
- [18] M. I. El-Hawwary and M. Maggiore, "Case studies on passivity-based stabilisation of closed sets," *International Journal of Control*, vol. 84, no. 2, pp. 336–350, 2011.
- [19] A. Hladio, C. Nielsen, and D. Wang, "Path following for a class of mechanical systems," *IEEE Trans. Control Syst. Tech.*, vol. 21, no. 6, pp. 2380–2390, Nov 2013.
- [20] A. Akhtar, C. Nielsen, and S. Waslander, "Path following using dynamic transverse feedback linearization for car-like robots," *IEEE Trans. Robotics*, vol. 31, no. 2, pp. 269–279, April 2015.
- [21] S. Kolyubin and A. Shiriaev, "Dynamics-consistent motion planning for underactuated ships using virtual holonomic constraints," in *Proc. of IEEE OCEANS 2014*, Sept 2014, pp. 1–7.
- [22] Y. Kapitanyuk and S. Chepinsky, "Control of mobile robot following a piecewise-smooth path," *Gyroscope and Navigation*, vol. 4, no. 4, pp. 198–203, 2013.
- [23] Y. Kapitanyuk, S. Chepinskiy, and A. Kapitonov, "Geometric path following control of a rigid body based on the stabilization of sets," in *Proc. of the 19th IFAC World Congress*, Cape Town, South Africa, 2014, pp. 7342–7347.
- [24] J. Wang, I. A. Kapitaniuk, S. A. Chepinskiy, D. Liu, and A. J. Krasnov, "Geometric path following control in a moving frame," *IFAC-PapersOnLine*, vol. 48, no. 11, pp. 150 – 155, 2015.
- [25] R. Gill, D. Kulić, and C. Nielsen, "Spline path following for redundant mechanical systems," *IEEE Trans. Robotics*, vol. 31, no. 6, pp. 1378–1392, 2015.
- [26] D. Panagou and V. Kumar, "Cooperative visibility maintenance for leader-follower formations in obstacle environments," *IEEE Trans. Robotics*, vol. 30, no. 4, pp. 831–844, 2014.
- [27] M. Hoy, A. Matveev, and A. V. Savkin, "Algorithms for collision-free navigation of mobile robots in complex cluttered environments: a survey," *Robotica*, vol. 33, no. 3, pp. 463–497, 2015.
- [28] D. A. Lawrence, E. W. Frew, and W. J. Pisano, "Lyapunov vector fields for autonomous unmanned aircraft flight control," *Journal of Guidance, Control, and Dynamics*, vol. 31, no. 5, pp. 1220–1229, 2008.

- [29] D. Nelson, D. Barber, T. McLain, and R. Beard, "Vector field path following for miniature air vehicles," *IEEE Trans. Robotics*, vol. 23, no. 3, pp. 519–529, June 2007.
- [30] L. Valbuena Reyes and H. Tanner, "Flocking, formation control, and path following for a group of mobile robots," *IEEE Trans. Control Syst. Tech.*, vol. 23, no. 4, pp. 1268–1282, July 2015.
- [31] V. Goncalves, L. Pimenta, C. Maia, B. Dutra, and G. Pereira, "Vector fields for robot navigation along time-varying curves in  $n$ -dimensions," *IEEE Trans. Robotics*, vol. 26, no. 4, pp. 647–659, Aug 2010.
- [32] R. Beard, J. Ferrin, and J. Humpherys, "Fixed wing uav path following in wind with input constraints," *IEEE Trans. Control Syst. Tech.*, vol. 22, no. 6, pp. 2103–2117, Nov 2014.
- [33] T. I. Fossen, *Guidance and control of ocean vehicles*. John Wiley & Sons, Ltd, 1994.
- [34] R. W. Beard and T. W. McLain, *Small unmanned aircraft: Theory and practice*. Princeton university press, 2012.
- [35] A. Tsourdos, B. White, and M. Shanmugavel, *Cooperative Path Planning of Unmanned Aerial Vehicles*, ser. Aerospace Series. Wiley, 2010.
- [36] T. I. Fossen, K. Y. Pettersen, and R. Galeazzi, "Line-of-sight path following for Dubins paths with adaptive sideslip compensation of drift forces," *IEEE Trans. Control Syst. Tech.*, vol. 23, no. 2, pp. 820–827, 2015.
- [37] P. Morin and C. Samson, "Trajectory tracking for non-holonomic vehicles: overview and case study," in *Proc. of 4th Int. Workshop on Robot Motion and Control RoMoCo'04.*, June 2004, pp. 139–153.
- [38] G. Oriolo, A. D. Luca, and M. Vendittelli, "WMR control via dynamic feedback linearization: Design, implementation, and experimental validation," *IEEE Trans. Control Syst. Tech.*, vol. 10, no. 6, pp. 835–852, 2002.
- [39] H. Khalil, *Nonlinear systems*. Englewood Cliffs, NJ: Prentice-Hall, 1996.
- [40] F. Mondada, M. Bonani, X. Raemy, J. Pugh, C. Cianci, A. Klapotcz, S. Magnenat, J.-C. Zufferey, D. Floreano, and A. Martinoli, "The e-puck, a robot designed for education in engineering," in *Proc. of the 9th Conf. on Auton. Robot Syst. and Competitions*, 2009, pp. 59–65.